(Received 10 March 2024, Accepted 16 April 2024, Scheduled 25 April 2024)

Broadband AMC Metasurface and Its Application for Radar Cross Section Reduction of a Microstrip Antenna

Xutong Wang[1,2], Liping Han[1,2,*], Guorui Han[1,2], Yufeng Liu[1,2], and Yanfeng Geng[1,2]

[1] School of Physics and Electronic Engineering, Shanxi University, Taiyuan 030006, China
[2] Electronics Technology Group Corporation, Taiyuan 030006, China

ABSTRACT: A broadband artificial magnetic conductor (AMC) metasurface for radar cross section reduction is proposed. Modified Jerusalem cross unit and quasi-circular unit can achieve effective reflection phase difference of $180°(\pm 37°)$ within a wide frequency range from 8.95 to 17.3 GHz. The broadband metasurface consists of chessboard-arranged 3×3 block arrays, and each block array is composed of 4×4 AMC units. The proposed AMC metasurface is applied to a microstrip antenna for reducing RCS. The measurement results show that the low RCS antenna can obtain 10 dB RCS reduction from 7.93 to 17.5 GHz. The relative bandwidth is 75.2%, and the maximum reduction value is 30.2 dB. Also, radiation performance of the antenna is well maintained.

1. INTRODUCTION

With the rapid development of radar detection technology, the modern warfare landscape has become complex [1]. To meet the growing demand for stealth capabilities of aircraft, ships, and other platforms, radar cross section (RCS) reduction of targets has attracted much attention of researchers [2]. Microstrip antennas with the characteristics of effective reception and radiation of electromagnetic wave energy play a crucial role in RCS reduction [3]. The traditional RCS reduction methods are shape modification technique [4] and coating with absorbing materials on the target surface [5, 6]. The former method usually leads to poorer stealth effect, and the latter method causes deterioration in the antenna radiation performance. Metasurface is a novel type of material. Metasurface is widely applied to improve antenna performance and RCS reduction because it can flexibly control the amplitude, phase, and polarization of incident waves [7]. Therefore, more effective RCS reduction without deteriorating its radiation performance is still a tough challenge [8].

In recent years, a lot of metasurfaces for RCS reduction of antennas have been proposed, such as coding metasurface [9], polarization conversion metasurface [10, 11], and AMC metasurface [12–14]. In [9], a microstrip antenna loaded with a novel coding metasurface is proposed. The 10 dB RCS reduction relative bandwidth is 17.3%. In [10], a polarization conversion metasurface with curved square-ring elements is arranged around a radiating patch. The relative bandwidth is 7.05%. In [11], a polarization conversion metasurface is applied to a multiple-input multiple-output (MIMO) slot antenna achieving 10 dB reduction with a 35.3% bandwidth. In [12–14], the RCS of the proposed antenna is reduced by using a metasurface composed of two different AMC units. The 10 dB RCS reduction bandwidths can reach 57.1%, 65.2%, and 71.6%, respectively. In the above mentioned antennas, the antennas with more than 50% reduction bandwidth have higher profiles. The aim of this paper is to design an antenna of lager RCS reduction bandwidth with lower profile.

In this paper, two different AMC units are presented, which can achieve effective reflection phase difference of $180°(\pm 37°)$ within a frequency range. A broadband metasurface is composed of 3×3 AMC block arrays. The metasurface is applied in a microstrip antenna to RCS reduction. The proposed antenna is verified, and the experiment indicates that the RCS reduction of 10 dB has been achieved across a wider frequency range. Meanwhile, the radiation performances of the antenna are good.

2. BROADBAND AMC METASURFACE

The RCS reduction principle of metasurface is that the scattered fields of the two AMCs cancel each other. When a plane wave is incident on a metasurface, the total reflection is

$$E_{\text{tr}} = 2E_{\text{i0}}e^{j\varphi_1}\left[1 + e^{j(\varphi_2-\varphi_1)}\right] \tag{1}$$

where E_{i0} is the incident fields acting on the AMCs, and φ_{i} is the reflection phase of AMCs. When the reflection phase difference is in the range from $143°$ to $217°$, the reflection energy of the AMCs would cancel each other.

2.1. AMC Unit Cells

The initial AMC structure is a Jerusalem cross and four circular patches with same size, and a phase difference with $180°(\pm 37°)$ is found in a narrow frequency region. A wide phase difference range of AMC structure is needed in this work. Figure 1 depicts the structure of the proposed AMC units. A modified Jerusalem cross structure and a quasi-circular structure are named as AMC1 and AMC2, respectively. The dimension of AMC unit is 10 mm $\times$ 10 mm. FR4 materials

* Corresponding author: Liping Han (hlp@sxu.edu.cn).

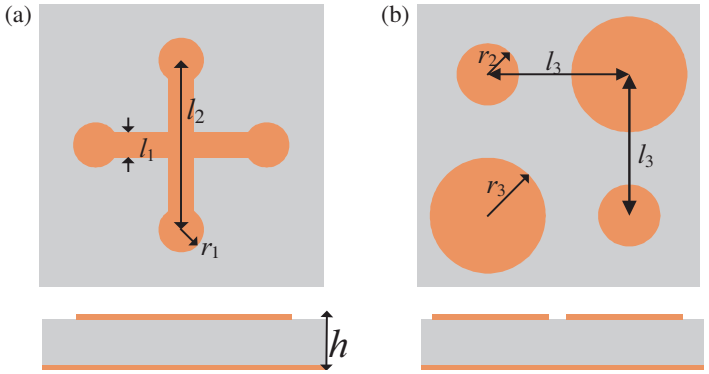

FIGURE 1. Structure of AMC unit cells. (a) AMC1, (b) AMC2.

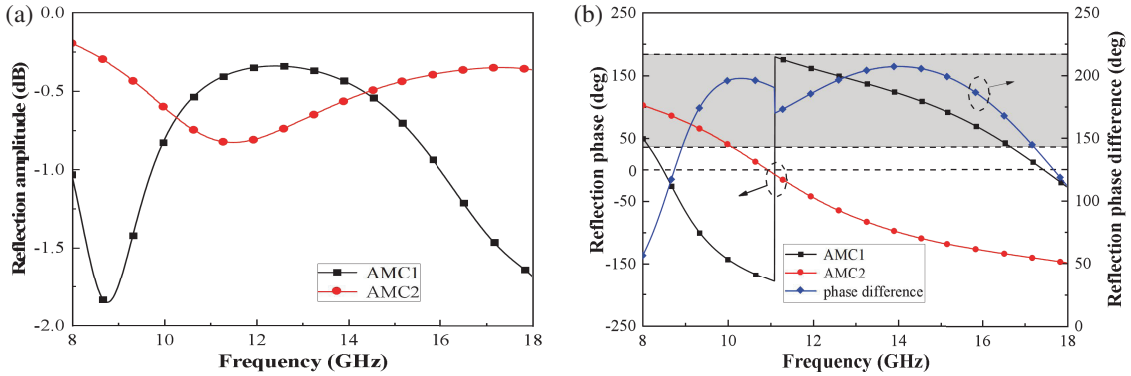

FIGURE 2. Reflection characteristics of AMC1 and AMC2. (a) Reflection amplitude, (a) reflection phases and phase difference.

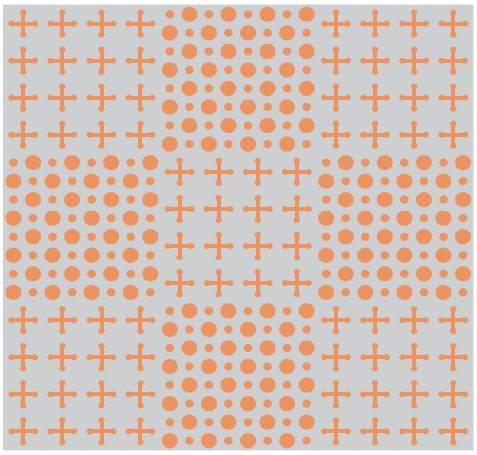

FIGURE 3. Configuration of AMC metasurface.

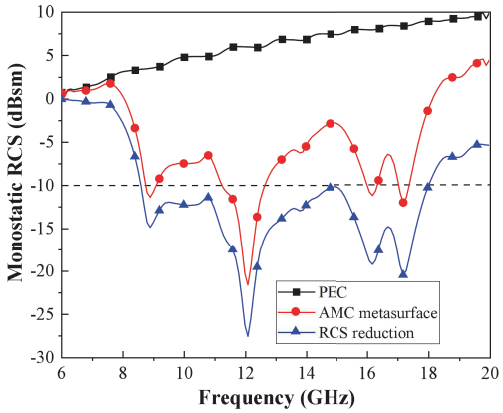

FIGURE 4. Monostatic RCS and RCS reduction.

with relative permittivity of 4.3 and dielectric loss of 0.025 are used as the substrate. The optimized parameters are as follows: $l_1 = 0.9\,\text{mm}$, $l_2 = 6\,\text{mm}$, $l_3 = 5\,\text{mm}$, $r_1 = 0.8\,\text{mm}$, $r_2 = 1.1\,\text{mm}$, $r_3 = 2.05\,\text{mm}$, $h = 2.4\,\text{mm}$.

The reflection characteristics of AMCs are shown in Figure 2. The reflection amplitudes of AMCs are less than $-1\,\text{dB}$ within a wideband as illustrated in Figure 2(a). It indicates that the incident energy is nearly reflected away instead of being absorbed. Figure 2(b) depicts the phase and phase difference of the AMC units, and the gray area in the figure represents the phase difference range from 143° to 217°. It is observed that AMC1 has 0° reflection phase at 8.5 GHz and 17.4 GHz and a reflection phase inverse point at 11.1 GHz. Also, AMC2 only exhibits a 0° reflection phase at 11.2 GHz, which is close to the reflection phase inverse point of AMC1. Therefore, AMC1 and AMC2 units exhibit a reflection phase difference of $180°(\pm 37°)$ within the range of 8.95–17.3 GHz. It indicates that the broadband RCS reduction can be achieved within the frequency range.

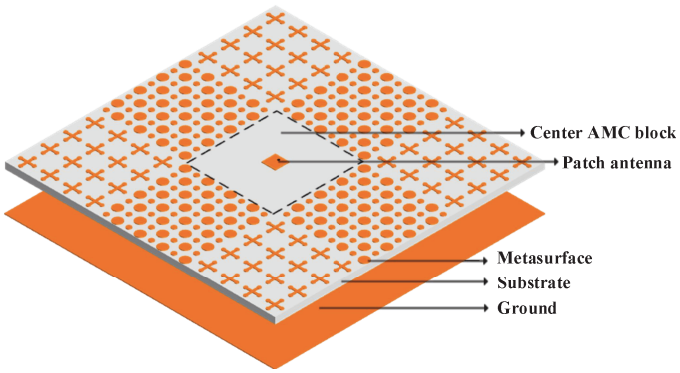

FIGURE 5. Configuration of the proposed antenna.

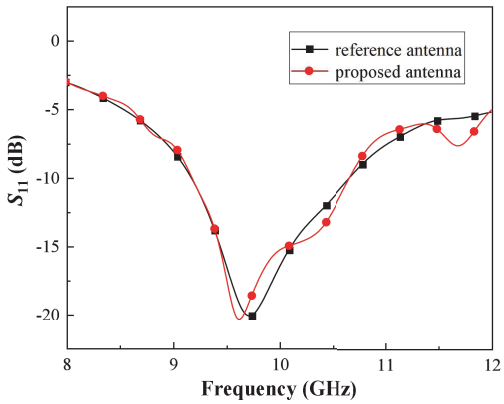

FIGURE 6. Simulated S_{11} of the antennas.

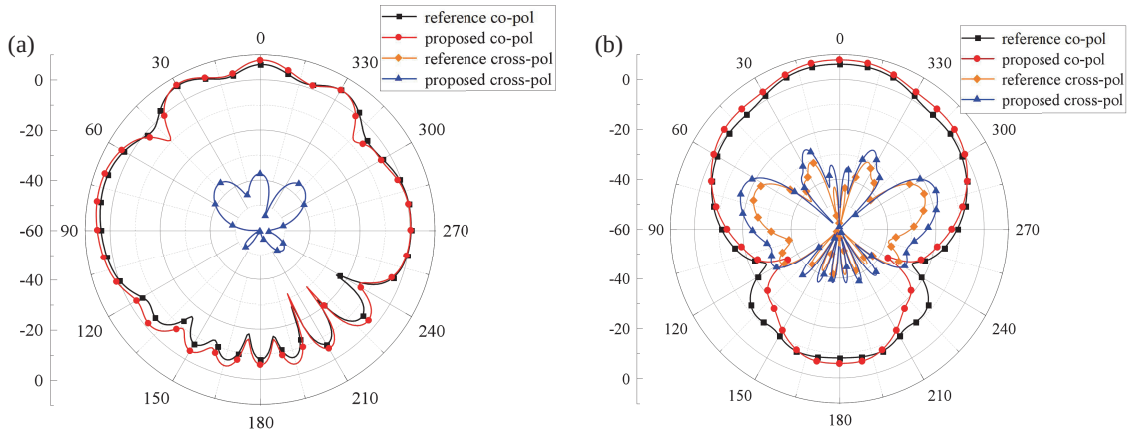

FIGURE 7. Simulated radiation patterns of the antennas at 10 GHz. (a) E-plane, (b) H-plane.

2.2. Broadband AMC Metasurface

The proposed metasurface structure consists of 3×3 block arrays, as shown in Figure 3. Each AMC block is composed of 4×4 AMC1 or AMC2, and the overall metasurface dimension is 120 mm $\times$ 120 mm. An ideal perfect electric conductor (PEC) of equal size to the metasurface is utilized as a reference structure. The monostatic RCS and RCS reduction results are illustrated in Figure 4. The AMC metasurface can obtain RCS reduction of 10 dB across the broad frequency range spanning from 8.6 to 18 GHz. The maximum RCS reduction is 27.6 dB.

3. LOW RCS ANTENNA BASED ON AMC METASURFACE

3.1. Configuration of the Proposed Antenna

The proposed antenna structure is depicted in Figure 5. The antenna configuration consists of the AMC metasurface and a patch antenna. To avoid impacting the radiation characteristics of the antenna, the center 4×4 AMC block of the metasurface is removed to place the radiating patch. The parameters of the AMC metasurface are the same as those of the aforementioned metasurface, and the dimension of the radiating patch is 6.15 mm $\times$ 6.15 mm. The position of the feed point is $x = 1.4$ mm from the center of the AMC block. Besides, an antenna without AMC metasurface is used as a reference antenna.

3.2. Radiation Performance of the Antenna

Figure 6 provides the simulated S_{11} of the antennas. The simulated bandwidth of the proposed antenna covers the frequency from 9.18 to 10.67 GHz. Compared with the reference antenna, the operation bandwidth of the proposed antenna is well kept. However, the resonant frequency of the proposed antenna is slightly shifted to the lower frequency by 0.1 GHz. The radiation patterns of the proposed and reference antennas in the E- and H-planes at 10 GHz are presented in Figure 7. It is obvious that the main lobes of the antennas are all along the normal direction. In conclusion, the antenna maintains excellent radiation properties after incorporating metasurface.

3.3. Radar Cross Section Reduction of the Antenna

To further validate the broadband scattering properties of the proposed antenna, Figure 8 shows the simulated monostatic RCS results. It can be seen that the 10 dB RCS reduction can reach a 69.4% bandwidth in a broad range of 8.65–17.85 GHz. The maximum RCS reduction is 23 dB. Figure 9 presents the simulated bistatic RCS results. In comparison to the reference

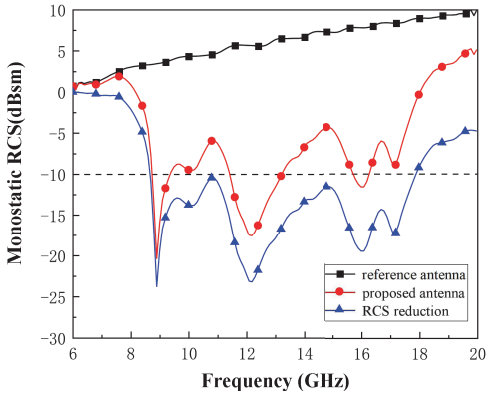

FIGURE 8. Monostatic RCS and RCS reduction.

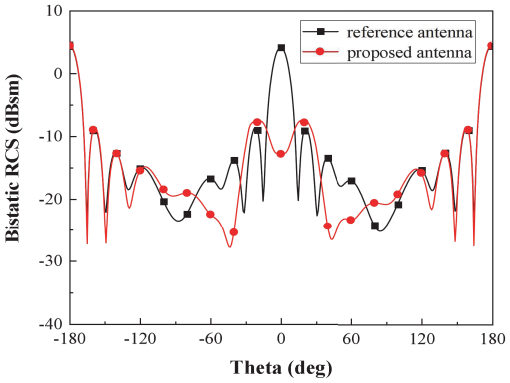

FIGURE 9. Bistatic RCS of the proposed and reference antennas.

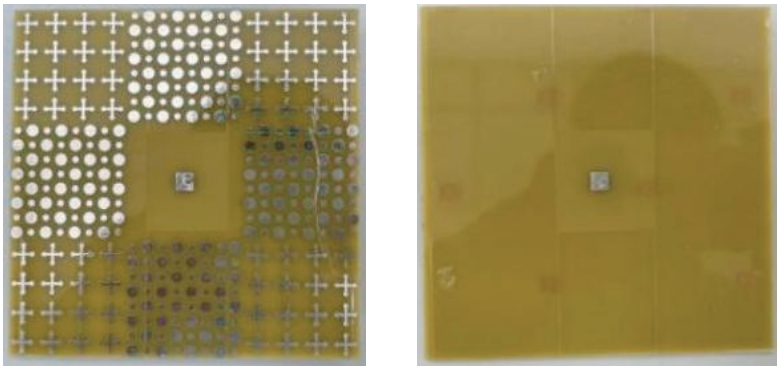

FIGURE 10. Photographs of the fabricated and measured environment. (a) Proposed antenna, (b) reference antenna.

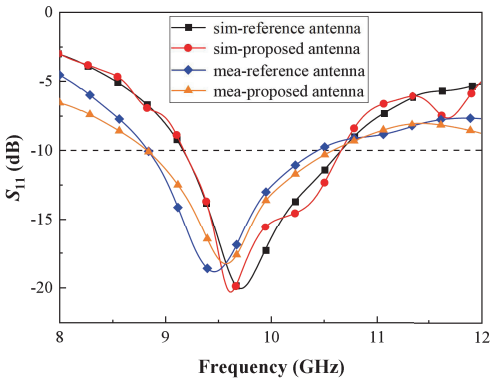

FIGURE 11. Simulated and measured S_{11} of the antennas.

TABLE 1. Comparative performance of the proposed and existing or reported antennas.

Refs.	Size (λ_0^3)	Frequency (GHz)	10 dB RCSR BW (%)	IBW (%)	Max reduction (dB)
Ref. [9]	$0.90 \times 0.90 \times 0.050$	8.15–9.7	17.3	2.8	32
Ref. [10]	$1.15 \times 1.15 \times 0.029$	4.1–4.4	7.05	2.6	24
Ref. [11]	$1.67 \times 1.67 \times 0.145$	5.6–8	35.3	6.4	25
Ref. [12]	$2.56 \times 2.56 \times 0.950$	9.5–18	61.8	31.6	35
Ref. [13]	$2.83 \times 2.83 \times 0.104$	8.8–17.3	65.2	15.4	32
Ref. [14]	$2.84 \times 2.84 \times 0.105$	8.5–18	71.7	16.3	40
Proposed work	$4.00 \times 4.00 \times 0.080$	7.93–17.5	75.2	18.2	30.2

antenna, it can be seen that the RCS reduction of the proposed antenna is realized from $-15°$ to $+15°$.

4. EXPERIMENTAL RESULTS

An Agilent N5221A vector network analyzer is used to measure the reflection coefficients, and an automatic antenna measurement system is used to measure the radiation patterns of the antennas. Photographs of the fabricated proposed and reference antennas are presented in Figures 10(a) and (b), respectively.

The simulated and measured S_{11} of the proposed and reference antennas are presented in Figure 11. It can be obtained that the measured results are roughly equal to the simulated ones. The measured operation bandwidths of the proposed and reference antennas are 8.84–10.46 GHz and 8.84–10.6 GHz, respectively. The measured resonant frequency of the antennas is shifted towards lower frequency, which is due to the deviation of manufacturing process and the substrate dielectric constant.

The simulated and measured radiation patterns of the antennas are illustrated in Figures 12(a)–(d). It is obvious that the simulated radiation patterns agree well with the measured ones. The main lobes of the antennas E- and H-planes are all along normal direction. The E-plane cross polarizations of the antennas are less than -21 dB and -18 dB, respectively. Also,

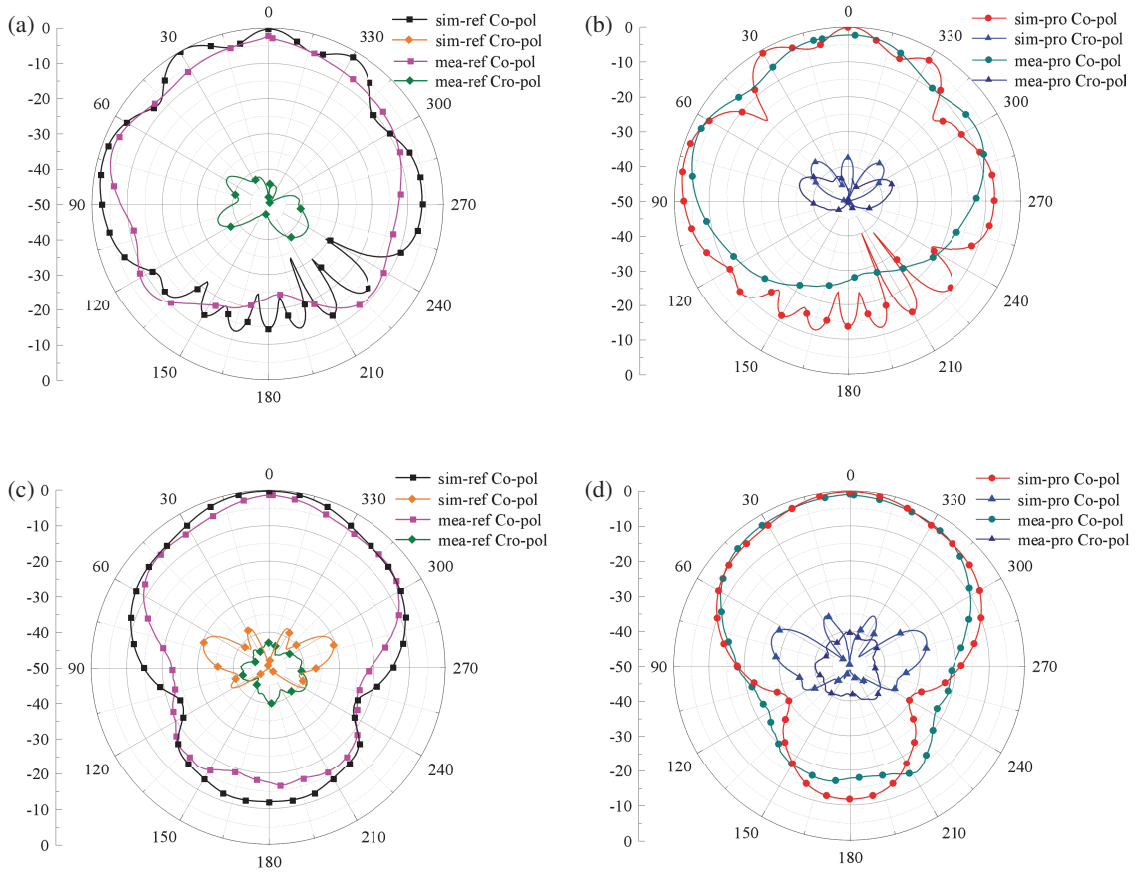

FIGURE 12. Simulated and measured radiation patterns of the antennas. E-plane: (a) reference and (b) proposed. H-plane: (c) reference and (d) proposed.

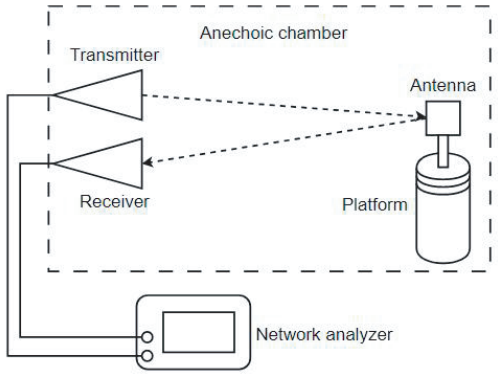

FIGURE 13. Schematic view of the RCS measurement setup.

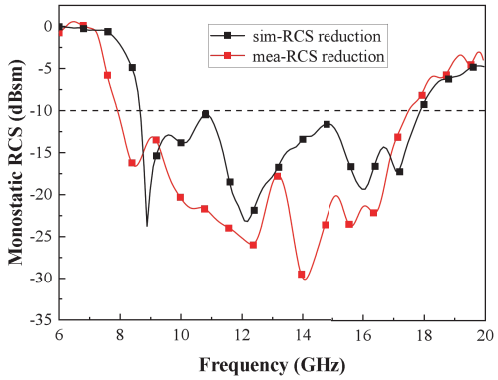

FIGURE 14. Simulated and measured RCS reduction of the antennas.

the H-plane cross polarizations of the antennas are less than -21 dB and -18 dB, respectively.

To further verify the RCS reduction, schematic view of the RCS measurement setup is shown in Figure 13. Two horn antennas are connected to the Agilent N5221A network analyzer. One horn antenna is used as transmitter, and the other horn antenna is used to receive scattered signal generated by the testing antenna.

Figure 14 presents the simulated and measured RCS reduction of the antennas. It can be seen that the measured and simulated results of RCS reduction are basically similar. The measured results show that the 10 dB RCS reduction bandwidth can obtain from 7.93 to 17.5 GHz (75.2%). The maximum reduction is 30.2 dB at 14.1 GHz. Due to fabrication and measurement tolerance, there are slight discrepancies between the measured and simulated results.

Table 1 lists the comparison of the proposed and reported antennas. It can be seen that the proposed antenna possesses the broadest 10 dB RCS reduction bandwidth, and the impedance bandwidth is the largest except the antenna in [12]. The overall dimension of the proposed antenna is reduced by 79.5% compared with the antenna in [12]. Compared to the antennas with

larger reduction bandwidth [13, 14], the profile of the antenna in this work is reduced by 23.1% and 23.8%, respectively.

5. CONCLUSIONS

In this paper, the modified Jerusalem cross and quasi-circular units with a reflection phase difference of $180°(\pm 37°)$ in a wide range are proposed. Nine block arrays composed of AMC units are arranged to form the broadband AMC metasurface. RCS reduction of microstrip antenna is obtained via loading the AMC metasurface. The proposed antenna is validated with simulation and measurement. The results indicate that the proposed antenna can achieve 10 dB RCS reduction within the frequency range of 7.93–17.5 GHz (75.2%).

ACKNOWLEDGEMENT

This work was supported by the National Natural Science Foundation of China (62071282, 61771295) and Fundamental Research Program of Shanxi Province (202303021221072).

REFERENCES

[1] Sharma, A., D. Gangwar, B. K. Kanaujia, S. Dwari, and S. Kumar, "Design of a wideband polarisation conversion metasurface and its application for RCS reduction and gain enhancement of a circularly polarised antenna," *IET Microwaves, Antennas & Propagation*, Vol. 13, No. 9, 1427–1437, 2019.

[2] Samadi, F. and A. Sebak, "Wideband, very low RCS engineered surface with a wide incident angle stability," *IEEE Transactions on Antennas and Propagation*, Vol. 69, No. 3, 1809–1814, 2021.

[3] Thummaluru, S. R., R. Kumar, and R. K. Chaudhary, "Isolation enhancement and radar cross section reduction of MIMO antenna with frequency selective surface," *IEEE Transactions on Antennas and Propagation*, Vol. 66, No. 3, 1595–1600, 2018.

[4] Rajesh, N., K. Malathi, S. Raju, V. A. Kumar, S. D. R. Prasath, and M. G. N. Alsath, "Design of Vivaldi antenna with wideband radar cross section reduction," *IEEE Transactions on Antennas and Propagation*, Vol. 65, No. 4, 2102–2105, 2017.

[5] Chen, W., C. A. Balanis, and C. R. Birtcher, "Checkerboard EBG surfaces for wideband radar cross section reduction," *IEEE Transactions on Antennas and Propagation*, Vol. 63, No. 6, 2636–2645, 2015.

[6] Modi, A. Y., C. A. Balanis, C. R. Birtcher, and H. N. Shaman, "Novel design of ultrabroadband radar cross section reduction surfaces using artificial magnetic conductors," *IEEE Transactions on Antennas and Propagation*, Vol. 65, No. 10, 5406–5417, 2017.

[7] Cheng, Y.-F., J. Feng, C. Liao, and X. Ding, "Analysis and design of wideband low-RCS wide-scan phased array with AMC ground," *IEEE Antennas and Wireless Propagation Letters*, Vol. 20, No. 2, 209–213, 2021.

[8] Abdullah, M. and S. Koziel, "Supervised-learning-based development of multibit RCS-reduced coding metasurfaces," *IEEE Transactions on Microwave Theory and Techniques*, Vol. 70, No. 1, 264–274, 2022.

[9] Pazokian, M., N. Komjani, and M. Karimipour, "Broadband RCS reduction of microstrip antenna using coding frequency selective surface," *IEEE Antennas and Wireless Propagation Letters*, Vol. 17, No. 8, 1382–1385, 2018.

[10] Liu, Y., Y. Hao, K. Li, and S. Gong, "Radar cross section reduction of a microstrip antenna based on polarization conversion metamaterial," *IEEE Antennas and Wireless Propagation Letters*, Vol. 15, 80–83, 2015.

[11] Pandit, S., A. Mohan, and P. Ray, "Low-RCS low-profile four-element MIMO antenna using polarization conversion metasurface," *IEEE Antennas and Wireless Propagation Letters*, Vol. 19, No. 12, 2102–2106, 2020.

[12] Xing, Z., F. Yang, P. Yang, and J. Yang, "A low-RCS and wideband circularly polarized array antenna co-designed with a high-performance AMC-FSS radome," *IEEE Antennas and Wireless Propagation Letters*, Vol. 21, No. 8, 1659–1663, 2022.

[13] Zheng, Y., J. Gao, X. Cao, Z. Yuan, and H. Yang, "Wideband RCS reduction of a microstrip antenna using artificial magnetic conductor structures," *IEEE Antennas and Wireless Propagation Letters*, Vol. 14, 1582–1585, 2015.

[14] Zheng, Y.-J., J. Gao, Y.-L. Zhou, X.-Y. Cao, L.-M. Xu, S.-J. Li, and H.-H. Yang, "Metamaterial-based patch antenna with wideband RCS reduction and gain enhancement using improved loading method," *IET Microwaves, Antennas & Propagation*, Vol. 11, No. 9, 1183–1189, 2017.